Eur. Phys. J. D **7**, 89–97 (1999)

THE EUROPEAN PHYSICAL JOURNAL D

EDP Sciences

Structural characterization of pumice-supported silver-palladium metal clusters by means of XAFS and AWAXS

A. Balerna[1,a], L. Liotta[2], A. Longo[2,3] A. Martorana[2,3] C. Meneghini[1], S. Mobilio[1,4], and G. Pipitone[2,3]

[1] Istituto Nazionale di Fisica Nucleare, Laboratori Nazionali di Frascati, Via E. Fermi, 40, 00044 Frascati, Italy
[2] Istituto di Chimica e Tecnologia dei Prodotti Naturali del CNR, Via Ugo La Malfa, 153, 90146 Palermo, Italy
[3] Dipartimento di Chimica Inorganica, Università di Palermo, Via Archirafi, 26, 90123 Palermo, Italy
[4] Dipartimento di Fisica, Università di Roma Tre, Via della Vasca Navale, 84, 00146 Roma, Italy

Received: 21 December 1998 / Received in final form: 19 March 1999

Abstract. Silver-palladium bimetallic clusters were synthesized on pumice by the reduction of aqueous solution of metal salts with different Pd:Ag ratios. Used as bimetallic catalysts, in hydrogenation reactions, in situations where molecules can undergo several different reactions, they eliminate undesired reactions and maximize the desired ones. To characterize the structure of these bimetallic catalysts and control if the two metallic elements do mix or not to each other to form an alloy, the structure of the Ag-Pd bimetallic clusters was investigated by means of X-ray-absorption fine-structure spectroscopy (XAFS) and anomalous wide angle X-ray scattering (AWAXS) experiments performed at the European Synchrotron Radiation Facility (ESRF) using the GILDA and the BM16 beamlines. A correlation between Ag and Pd was found but not a clear evidence of alloying.

PACS. 61.10.-i X-ray diffraction and scattering – 61.10.Ht X-ray absorption spectroscopy: EXAFS, NEXAFS, XANES, etc. – 61.43.Gt Powders, porous materials

1 Introduction

The hydrogenation of highly unsaturated hydrocarbons is of great industrial importance. Indeed, small concentrations of alkynes and alkadienes must be removed from C2, C3 and C4 alkenes feedstocks before they can be processed by polymerization [1,2]. Palladium is the most active and selective metal for these kinds of reactions. Nevertheless its use involves several drawbacks: the selectivity is restricted by competitive reactions such as the complete hydrogenation of the hydrocarbon and the isomerization of the diolefins containing more than 3 carbon atoms. Several attempts have been made to minimize these undesired side reactions by using bimetallic catalysts [3,4]. Different synthetic strategies have been used for the production of such multimetallic clusters [5,6] sometimes favouring alloying [5], sometimes the growth of monometallic clusters [6]. In particular Pd-Ag bimetallic catalysts [7] have shown better performances than monometallic palladium probably due to the modified chemical environment of the Pd atoms [8] induced by the presence of Ag.

In this paper, the structural characterization of bimetallic Pd-Ag catalysts, supported on pumice, is reported, showing that a correlation exists between the Ag and Pd atoms.

[a] e-mail: balerna@lnf.infn.it

In order to perform this structural investigation X-ray Absorption Fine Structure (XAFS) spectroscopy was used to investigate the short-range order characteristics around the Ag and Pd atoms, while Anomalous Wide Angle X-ray Scattering (AWAXS) was used to investigate the long-range ones.

2 Experimental

The pumice from the island of Lipari (Italy) is an amorphous volcanic alumino-silicate whose atomic structure [9] is not very different from that of amorphous silica, a compound often used as a carrier for heterogeneous catalysts, expecially when synthesized as a high surface area material. Despite its very low specific surface area (about 1 m^2/g, according to small angle X-ray scattering data analysis [9]), pumice has been successfully employed in the synthesis of monometallic Pd [10], Rh [11] and Ni [12] catalysts; this reported good efficiency has been demonstrated to depend on the presence of sodium-bearing species in the support framework [13], that modify the electronic properties of the supported metal, and on the transport of reactants and products favoured by the small surface area.

The Ag-Pd metal clusters were supported on pumice using the following synthesis technique [8]:

i) impregnation of pumice with $[Pd(NH_3)_4](NO_3)_2$ and, subsequently, with $[Ag(NH_3)_2]NO_3$ metal salts in aqueous solution with different Ag:Pd ratios; ii) calcination at 773 °C, 1 atm O_2; iii) reduction at 623 °C, 1 atm. Two monometallic reference samples and three bimetallic Pd_xAg_y samples with different Pd and Ag concentrations were prepared. The Pd and Ag content in the samples was determined by atomic absorption with a relative error of about 10%. The bimetallic samples are: sample **A** with $x = 0.25$ wt.%, $y = 0.08$ wt.%, sample **B** with $x = 0.17$ wt.%, $y = 0.07$ wt.% and sample **C** with $x = 0.25$ wt.%, $y = 0.05$ wt.%. The monometallic ones are: sample **D** with $x = 0$, $y = 0.05$ wt.% and sample **E** with $x = 0.2$, $y = 0$ wt.%.

The XAFS measurements at the Ag (25.514 kev) and Pd (24.350 kev) K-edges were performed at the European Synchrotron Radiation Facility (ESRF) on the Italian beamline GILDA [14]. Beam energies were defined using a Si(311) double crystal monochromator that gives a resolution of about 1.5 eV at these energies. The dynamical sagittal focusing of GILDA monochromator [15] allowed to focus 4 mrad of the orizontal beam divergence to achieve a small (2 mm) and intense (10^{11} ph/s) spot at the sample. This configuration is particularly suited for fluorescence XAFS measurements on diluted samples where high photon fluxes are required. Harmonic rejection was achieved using two Pt coated mirrors (energy cut-off at $\sim$ 27 keV) which also focus the beam in the vertical direction.

The samples for the XAFS measurements were prepared by suspending the fine powder of the pumice supported samples in ethylic alcohol and depositing it on millipore membranes under N_2 atmosphere, to avoid any oxidation from air.

The XAFS measurements were performed in transmission geometry, with two Ar-filled ionization chambers to detect the incident (I_0) and transmitted (I_t) beam, on three bulk Ag, Pd and Ag_2O reference samples and in fluorescence geometry on the pumice supported samples. The Ag and Pd K_α fluorescence intensities (I_f) excited by the primary beam were detected using a 7-element HP-Ge multidetector (MD) each covering an area of 100 mm^2. The MD energy resolution allows to select a specific K_α line over the background due to elastic, Compton and others fluorescence signals, improving the data quality. All the XAFS spectra were recorded at 77 K to reduce the thermal effect of disorder which damps the amplitude of the XAFS oscillations.

The AWAXS data were taken at the ESRF high-resolution powder diffraction BM16 beamline [16]. This beamline, built on a bending magnet, is optimised for carrying out powder crystallography to solve and refine crystal structures; it can be used in a wide range of material science applications including anomalous scattering studies. The beam energies are defined using a Si(111) double crystal monochromator. The diffracted intensity is detected using a 9-crystal analyzer stage (nine Ge(111) crystals separated by 2° intervals) that, coupled with the high collimation of the incident radiation, gives narrow instrumental broadening.

Three samples were investigated at BM16: sample **A**, a monometallic pumice-supported Pd sample used as reference, and a pure pumice sample. X-ray diffraction spectra were recorded at room temperature on the samples contained in thin-walled glass capillary (⌀1.5 mm) and spinned in order to accurately measure the diffraction intensities. The diffraction data were taken at three different wavelengths: far from both Ag an Pd K-edges (λ_{off}), at the Pd K-edge (λ_{Pd}) and at the Ag K-edge (λ_{Ag}). The Ag and Pd K-edge energy values were chosen at the inflection point of the absorption edges of the pumice-supported monometallic Ag and Pd samples. The wavelength calibration was performed with high accuracy refining the diffraction patterns of a c-Si standard powder sample which gave also an estimation of the instrumental broadening that was smaller than 0.01°. The off-edge wavelength was determined as $\lambda_{off} = 0.63586$ Å, whereas the K-edge ones were $\lambda_{Pd} = 0.50909$ Å and $\lambda_{Ag} = 0.48600$ Å, respectively. Data were collected in a continuous scanning mode to eliminate the dead times of conventional step measurements. The spectra were normalized, averaged and recalculated to an equal step size of 0.002°. Absorption effects were negligible due to the low absorption coefficients of the samples at the wavelengths used in the experiments. For the differential intensities determinations, the patterns were interpolated and put on the same $\sin\theta/\lambda$ scale.

3 Data analysis

3.1 XAFS data analysis

The X-ray absorption fine structure signal, $\chi(k)$, is given by the oscillations present in the absorption coefficient, $\mu(k)$, of an atom (absorbing center) in the region above its absorption edge. These oscillations, superimposed onto the smooth total atomic absorption coefficient μ_0, are linked to the local atomic arrangement around the absorbing center. The signal, $\chi(k)$, is defined as

$$\chi(k) = \frac{\mu(k) - \mu_0(k)}{\mu_0(k)},$$

where

$$k = \sqrt{\frac{2m}{\hbar^2}(E - E_0)}$$

is the modulus of the wave vector of the photoelectron created in the absorption process and E_0 is the energy value corresponding to the maximum derivative of the absorption coefficient at the edge.

To determine the local structure, XAFS spectra can be analysed using very different procedures; in this specific case the GNXAS package [17,18] was used. According to this approach, the contributions of the local atomic arrangement around the absorbing atom to the $\chi(k)$ signal are decomposed in terms of irreducible n-body contributions, "$\gamma^{(n)}$". Each $\gamma^{(n)}$ is calculated, within the multiple

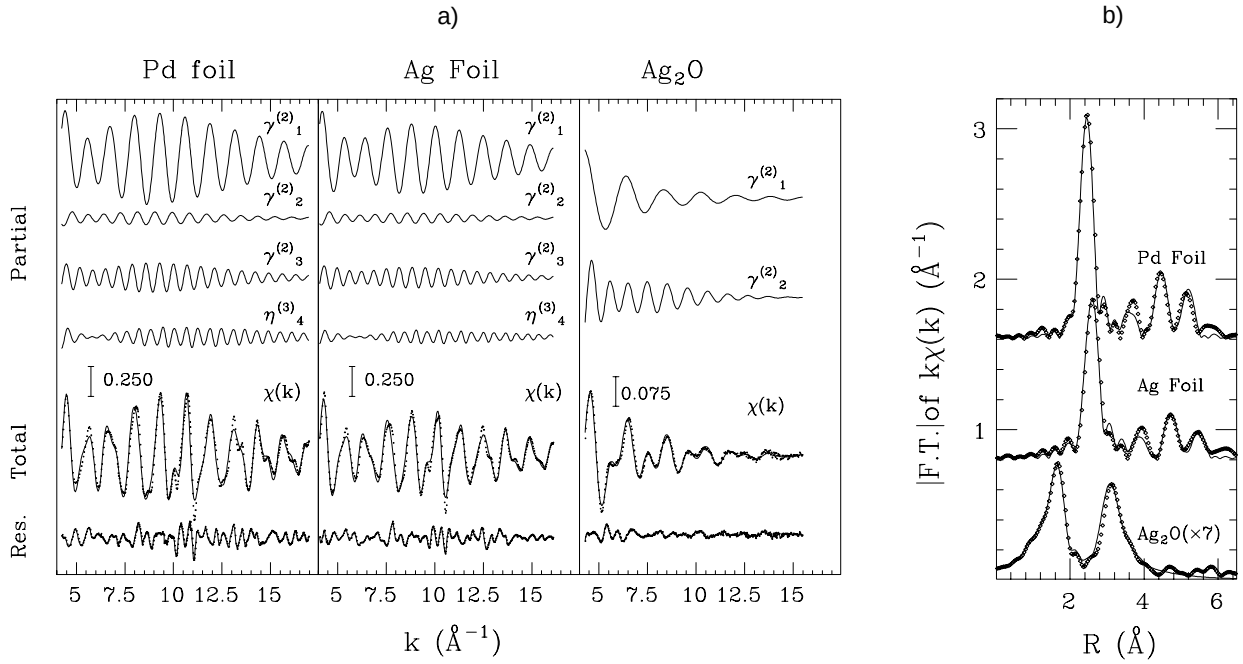

Fig. 1. a) Best fit of the XAFS spectra of the bulk reference samples. The different $k\chi(k)$ signals corresponding to pair contributions ($\gamma^{(2)}$) for the different coordination shells are shown as continuous lines. A continuous line indicates also the fourth shell contribution of the Ag and Pd foils where $\eta^{(3)} = \gamma^{(3)} + \gamma^{(2)}$ represents the three-body signal plus the fourth shell two-body one. In the lower part of the figure the comparison between the experimental data (dots) and the total theoretical signals (solid line), together with the residual experimental data are reported. b) k-weighted Fourier Transforms (FT) of the experimental (full lines) and theoretical (dots) $\chi(k)$ of the bulk reference samples.

scattering approach, considering all the contributions associated to a configuration of n-atoms, *i.e.* all the possible single and multiple scattering (MS) paths between the n-atoms. The use of complex Hedin-Lundqvist potentials permits a correct inclusion of the effects due to inelastic losses. GNXAS applies a fitting procedure directly on the experimental data carrying out a detailed error analysis on the fitting parameters to achieve a good estimate of the confidence interval on the final results. The statistical errors on parameters are evaluated according to the dimension of ellipses which encloses, in the parameter space, χ^2 values with a confidence of 95% [18].

In order to analyze the EXAFS spectra of the pumice-supported catalysts we had to analyze as first the EXAFS spectra of reference samples in order to evaluate and fix in the fitting procedures of the samples under study, amplitude parameters and phase shifts. The transferability of amplitudes and phase shifts between the reference samples and the ones under study requires similar chemical environments.

As reference samples crystalline Ag_2O, Ag and Pd were used and their $\gamma^{(n)}$ functions were generated up to about 6 Å. Figure 1a reports the fine structure spectra, $k\chi(k)$, of the three reference samples (dots) together with the best-fit data (full lines); in the lower part the residual is reported.

The experimental $k\chi(k)$ of Ag_2O was well reproduced by using only two single scattering contributions ($\gamma^{(2)}$) relative to the first coordination shell made of 2 oxygen atoms at 2.05 Å and the second coordination shell made of 6 Ag atoms at 3.33 Å. To reproduce the XAFS of the Ag and Pd foils, contributions up to the fourth shell were included. Due to the alignment of the first and fourth shell atoms, which enhances the multiple scattering contribution of the fourth fcc shell (focusing effect), for the first three shells only $\gamma^{(2)}$ signals were used while for the fourth

Table 1. Best fit parameters achieved from reference samples data fitting procedure.

Sample	Ag	Pd	Ag_2O
N_1	12	12	2
R_1(Å)	2.87 (1)	2.75 (1)	2.05 (1)
σ_1^2($\times 10^{-3}$Å^2)	2.1 (4)	1.6 (2)	2.5 (5)
N_2	6	6	6
R_2(Å)	4.04 (3)	3.86 (2)	3.33 (2)
σ_2^2($\times 10^{-3}$Å^2)	4.2 (5)	3.3 (4)	11.0 (7)
N_3	24	24	
R_3(Å)	5.00 (7)	4.78 (7)	
σ_3^2($\times 10^{-3}$Å^2)	5.0 (7)	3.9 (5)	
N_4	12	12	
R_4(Å)	5.74 (2)	5.49 (6)	
σ_4^2($\times 10^{-3}$Å^2)	5.0 (7)	3.7 (5)	
θ (degrees)	180 (2)	180 (3)	

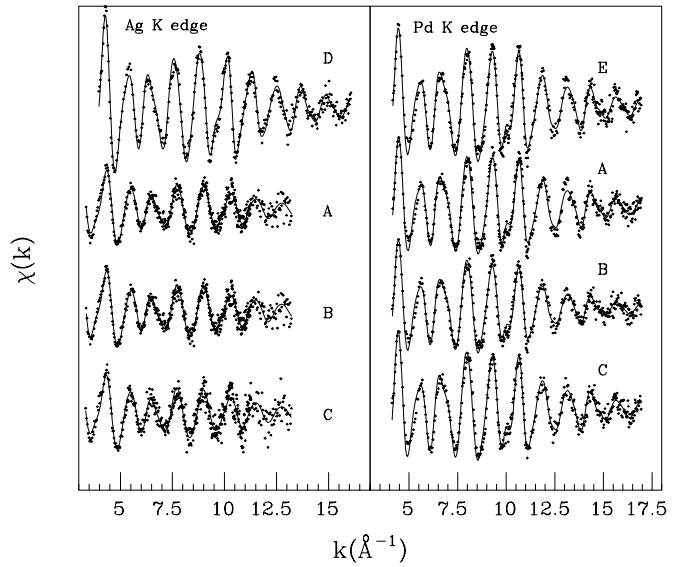

Fig. 2. Comparison between the experimental XAFS data (dots) and the total theoretical signals (solid line) of the bimetallic (**A**, **B**, **C**) and monometallic (**D**, **E**) pumice-supported samples taken at the Ag and Pd K-edges.

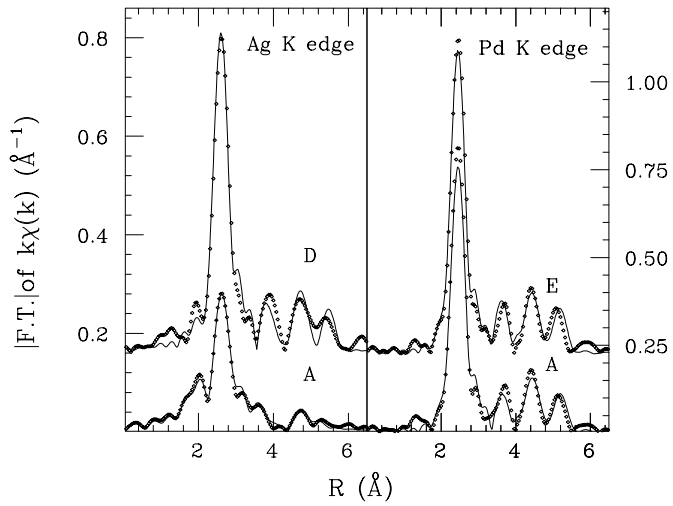

Fig. 3. k-weighted Fourier Transforms (FT) of the experimental (full lines) and theoretical (dots) $\chi(k)$ of one bimetallic (**A**) and of the two monometallic pumice-supported samples at the Ag and Pd K-edges.

one also a $\gamma^{(3)}$ contribution had to be included. Best fit parameters are reported in Table 1. The N values indicate the coordination numbers, R the nearest-neighbor (NN) interatomic distances and σ^2 the XAFS Debye-Waller factors. In Figure 1b the k-weighted Fourier Transforms (FT) of the experimental (full lines) and theoretical (dots) data are shown.

The values found for the reference samples are in agreement with the expected ones and this allowed to use the same local potentials in generating the $\gamma^{(n)}$ contributions for the XAFS spectra of the pumice-supported samples.

Figure 2 reports the experimental (dots) and theoretical (full lines) $\chi(k)$ of all the pumice-supported samples

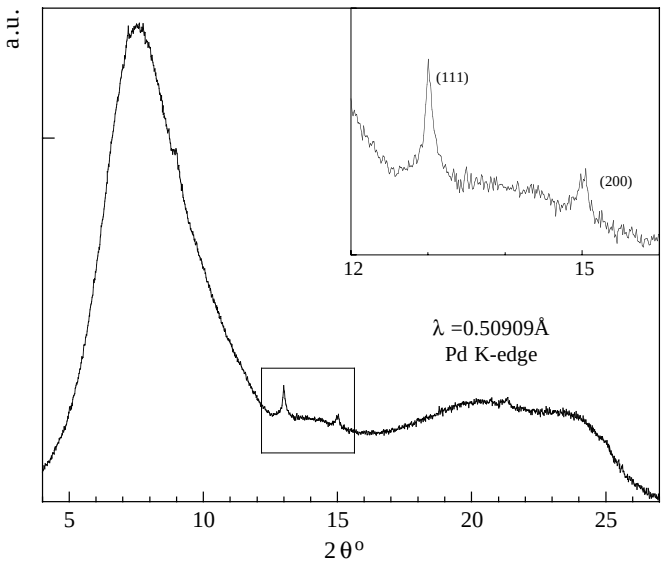

Fig. 4. WAXS spectra taken on sample **A** at $\lambda_{\rm Pd} = 0.50909$ Å. The (111) and (200) Pd diffraction peaks are clearly visible also if the total metal scattering is very low compared to that of the pumice support which gives the huge and wide halo in the low 2θ region and also the other smoother intensity features.

at the two different K-edges: due to the high dilution of the samples, the data quality is not as good as for the reference samples but still high enough to allow the analysis up to 16 Å^{-1} at the Pd K-edge and to 13 Å^{-1} at the Ag K-edge. To simulate the Pd K-edge data, the same contributions were required as in the bulk reference sample. At the Ag K-edge all the bulk contributions were necessary only for the monometallic Ag sample. For the bimetallic ones only single scattering, $\gamma^{(2)}$, signals related to the metallic phase had to be included together with an Ag-O contribution. This means that in these bimetallic samples Ag is present in two different phases: bound to other Ag atoms to form small clusters and bound to the O atoms of the pumice support. Best fit parameters are reported in Tables 2 and 3. Figure 3 shows the k-weighted FT of the monometallic pumice-supported reference samples and of one of the bimetallic samples (**A**); differences between bimetallic samples cannot be ruled out at this level. The big difference between the monometallic sample and the bimetallic one, at the Ag K-edge, is clearly visible in Figure 3.

3.2 AWAXS data analysis

Figure 4 shows the wide angle scattering pattern taken at the $\lambda_{\rm Pd}$ wavelength on sample **A**. The huge and wide halo and the other smooth and fainter intensity features are due to the pumice support. The (111) and (200) peaks are clearly visible, even if the total metal scattering is only a small fraction of the support one.

For a more reliable profile analysis, the pumice underlying intensity, measured at the $\lambda_{\rm off}$ wavelength, was

Table 2. Pumice-supported samples: best fit parameters achieved at the Pd K-edge.

Sample	**A**($y = 0.08$)	**B**($y = 0.06$)	**C**($y = 0.05$)	**E**($y = 0.00$)
N_1	10.2 (5)	10.3 (5)	10.9 (5)	11.1 (1)
R_1(Å)	2.75 (2)	2.75 (2)	2.75 (2)	2.75 (1)
$\sigma_1^2(\times 10^{-3}$Å$^2)$	3.7 (3)	3.8 (3)	3.7 (3)	3.6 (2)
N_2	4.2 (3)	4.3 (3)	4.8 (3)	4.9 (2)
R_2(Å)	3.87 (9)	3.87 (9)	3.87 (9)	3.87 (6)
$\sigma_2^2(\times 10^{-3}$Å$^2)$	5.0 (1.2)	4.7 (1.0)	4.0 (0.7)	3.3 (4)
N_3	15.0 (5)	16.0 (4)	19.1 (4)	17.2 (4)
R_3(Å)	4.77 (8)	4.77 (8)	4.77 (8)	4.77 (5)
$\sigma_3^2(\times 10^{-3}$Å$^2)$	6.2 (6)	7.0 (5)	6.2 (5)	6.2 (5)
N_4	10.0	10.0	10.8	11.1
(R_4(Å))	5.45 (9)	5.49 (7)	5.49 (7)	5.49 (7)
θ (degrees)	178 (3)	180 (2)	180 (2)	180 (3)

Table 3. Pumice-supported samples: best fit parameters achieved at the Ag K-edge.

Sample	**A**($y = 0.08$)	**B**($y = 0.06$)	**C**($y = 0.05$)	**D**($y = 0.05$)
Oxide phase				
Ag-O				
N_1	1.0 (7)	1.0 (7)	1.2 (8)	
R_1(Å)	2.26 (2)	2.27 (2)	2.26 (2)	
$\sigma_1^2(\times 10^{-3}$Å$^2)$	4.0 (6)	4.0 (6)	4.0 (7)	
Ag-Ag				
N_2	0.6 (8)	0.6 (8)	0.6 (9)	
R_2(Å)	3.57 (3)	3.56 (3)	3.57 (3)	
$\sigma_2^2(\times 10^{-3}$Å$^2)$	17.0 (6)	17.0 (6)	18.0 (8)	
Metallic phase				
Ag-Ag				
N_1	5.7 (5)	5.6 (5)	5.6 (6)	10.6 (4)
R_1(Å)	2.82 (3)	2.82 (3)	2.83 (4)	2.87 (2)
$\sigma_1^2(\times 10^{-3}$Å$^2)$	5.6 (5)	6.0 (5)	6.0 (6)	4.0 (5)
N_2	2.7 (6)	3.3 (6)	2.4 (7)	3.9 (5)
R_2(Å)	3.95 (5)	3.94 (5)	3.95 (6)	4.03 (5)
$\sigma_2^2(\times 10^{-3}$Å$^2)$	11.0 (5)	11.0 (6)	10.0 (6)	5.0 (5)
N_3	9.5 (7)	9.98 (7)	8.85 (8)	16.6 (6)
R_3(Å)	4.90 (5)	4.90 (5)	4.89 (6)	5.00 (6)
$\sigma_3^2(\times 10^{-3}$Å$^2)$	13.0 (6)	13.0 (6)	13.0 (7)	8.6 (6)
N_4				0.4
(R_4(Å))				5.74 (8)
θ (degrees)				177.7 (3.0)

subtracted from the **A** patterns after proper normalization.

In Figure 5 the (111) **A** sample diffraction peaks resulting from the pumice subtraction at the different exploited wavelengths are reported (dots) together with the corresponding pure Pd one taken far from the edge. The (111) diffraction peak of the monometallic Pd sample, due to the large clusters dimensions, is very narrow and also highly symmetric. On the contrary, in the Ag-Pd sample, the presence, in the low angle region, of a peak asymmetry is clearly visible. Since this asymmetry is not present in the (111) peak of the monometallic Pd sample, we exclude that it comes from instrumental effects (in particular, axial divergence [19]), and attribute this asymmetry to the presence of an additional contribution to the diffraction patterns.

As is well known, the simultaneous analysis of size-strain according to the Warren-Averbach procedure re-

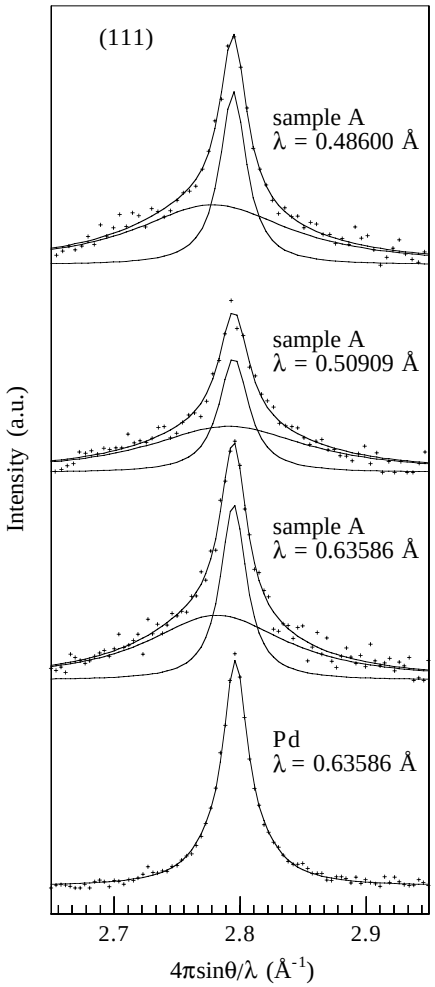

Fig. 5. Sample **A** (111) diffraction peaks (dots) recorded at different wavelengths and pure Pd (111) peak taken far from the edge (dots) together with their best fits indicated by a continuous line.

quires the availability of at least two reflections belonging to the same reciprocal lattice direction. For fcc structures, the first couple of peaks eligible for this treatment are the (111)-(222) ones; as can be seen from Figure 4, this is not suitable for our samples because the (222) reflection, at about 26.11°, is completely merged with the background. As a consequence, the (111) peak alone has been analyzed, attributing the peak broadening to size effects only and calculating the mean size as

$$\langle D \rangle^{-1} = - \lim_{D \to 0} \frac{\partial A(D)}{\partial D} ,$$

where $A(D)$ is the FT of the (111) peak profile [20]. This procedure gives an area-averaged mean cluster size that is underestimated due to the neglected disorder effects. A(D) has not been calculated from the rough data, but instead from a fitted analytical function [21]. The exploited one is constituted by the sum of two Lorentzian functions with independent width, position and amplitude. The choice is probably the most suitable as concerns: i) the correct asymptotic behavior as Q^{-2} [20]; ii) the good fitting to the experimental profiles, as reported in Figure 5 (full lines); iii) the use of the least number of parameters compatible with the thorough definition of a peak function. As already underlined, the evaluated instrumental broadening contribution to the FWHM was lower than 0.01° and therefore absolutely not relevant in the size determination. In Table 4 the most significant parameters so obtained are reported, together with the corresponding errors determined either by the minimization routine or by error propagation. The same analysis, performed on the DAWAXS (Differential Anomalous WAXS) pattern calculated from the couple constituted by the Pd-edge and off-edge catalyst data, gave similar results on a qualitative ground, but the worse signal-to-noise ratio gave rise to higher uncertainty in the fitting results.

4 Discussion

The aim of the present investigation was to evidence the presence of correlations between Ag and Pd in the bimetallic pumice-supported catalysts.

XAFS data ruled out interesting correlations and showed different environments for Ag and Pd. In both the monometallic samples the interatomic distances found were in agreement with the ones of the reference metallic foils. On the other hand, the coordination numbers and Debye-Waller factors were different from the bulk ones, showing the presence of small metal clusters. The reduction of the coordination numbers, N, can be used to estimate the average cluster sizes (D) [22]. Under the hypothesis of spherical cluster shape the values found are $D = 35$ Å for the monometallic Ag sample and $D = 60$ Å for the Pd one.

It is well known that a reduction of the N values could be given also by other causes. The nontransferability between the reference samples and the ones under study of an amplitude parameter like the electron mean free path can lead to an incorrect evaluation of the coordination numbers [23]. The same effect can be achieved if the presence of an asymmetric distance distribution, that could for some systems, like small clusters, result from the anharmonicity of the motion of the atoms located at the surface, is not taken into account [24]. As concerns the mean free path transferability, as reported in reference [23], for noble metals, as in our case, based on the experimental results that are a comparison between the D values achieved by electron microscopy and the ones deduced by the EXAFS coordination numbers, there is no evidence of a substantial change in the electron mean free path between the bulk and the small particles while in other cases, like Al and Fe, significant effects were found. Concerning possible effects of anharmonicity on the N values of these pumice-supported samples, we can stress that measurements were taken at 77 K and that the EXAFS data are k-weighted, so the high k EXAFS values are not emphasized. Moreover if the reduction effect at 100 K is extrapolated from reference [24], it is possible to show that it should be at least smaller than 5% which is in any case included in the 10% indetermination affecting the EXAFS N values.

Table 4. Structural analysis of the (111) peak of sample **A**.

	$\lambda_{\rm off} = 0.63586$ Å	$\lambda_{\rm Pd} = 0.50909$ Å	$\lambda_{\rm Ag} = 0.48600$ Å
Q_1[1]	2.788 (2)	2.794 (1)	2.786 (2)
Q_2[2]	2.7966 (2)	2.7968 (4)	2.7965 (2)
area$_1$[3]	71 (12)	57 (16)	73 (13)
area$_2$[4]	35 (4)	27 (4)	36 (4)
$(a^0)_1$[5]	3.903 (3)	3.895 (3)	3.906 (3)
$(a^0)_2$[6]	3.8914 (3)	3.8912 (6)	3.8916 (3)
D_1[7]	33 (3)	30 (4)	30 (3)
D_2[8]	183 (13)	158 (15)	177 (12)

[1] $Q_1 = 4\pi \sin\theta_1/\lambda$, peak position in Q units (Å^{-1}) of the first Lorentzian component.
[2] $Q_2 = 4\pi \sin\theta_2/\lambda$, position in Q units (Å^{-1}) of the second Lorentzian component.
[3] Area of the fitted first Lorentzian component.
[4] Area of the fitted second Lorentzian component.
[5] fcc cell constant (Å) as determined from Q_1.
[6] fcc cell constant (Å), as determined from Q_2.
[7] Average diameter (Å) related to the first Lorentzian component.
[8] Average diameter (Å) related to the second Lorentzian component.

In the case of the bimetallic samples, the Pd environment was found to have the same local structure as the monometallic sample, within the errors. The smaller coordination numbers are indicative of cluster diameters smaller than in the monometallic case, with values between 30 Å and 50 Å. Carefully observing Table 2, it could be recognized that the coordination numbers of the first three coordination shells in samples **A** and **B**, with a Ag:Pd ratio of about 1:3, are similar even if the Pd percentages are quite different; on the other hand, sample **C**, having a 1:5 Ag:Pd ratio, shows higher N values, although the Pd content is the same as in sample **A**. This behaviour is likely due to an interaction between Ag and Pd which has the effect of inhibiting the growth of large Pd clusters; however, there is no evidence, from the analysis of the Pd K-edge, of the existence of an appreciable amount of Pd-Ag bonds. In fact, the inclusion of Ag among the Pd neighbors in the fitting procedure did not improve the best fit quality.

The interpretation of the bimetallic samples data taken at the Ag K-edge is more complicated than the Pd one since, as shown in Table 3, in this case there is not only a reduction of the N values and an increase of the σ^2 ones but also a reduction of the metal-metal interatomic distance takes place. Another big difference compared to the Pd case is that Ag atoms are present in two different phases: bound to other Ag atoms to form small Ag clusters and a smaller part bound to the oxygen atoms of the pumice support. The Ag-O distances found in all samples are 0.2 Å longer than that in Ag_2O, indicating weaker bonds than in the oxide case because we are not dealing with a real oxidation but only with an interaction between the metal and the oxygen atoms belonging to the support. The R values are in agreement with other XAFS studies on metal clusters implanted in silica [25], on silver ions in different matrices [26] and Rh on alumina catalysts [27].

Due to the presence of these two phases, it is not possible to use the same procedure as in the Pd case to evaluate the Ag cluster dimensions; in fact in this case the N value found for a specific neighboring atom is not the real coordination number ($N_{\rm th}$) but is weighted by the atomic percentage, α, of Ag atoms present in that phase, *i.e.*

$$N = \alpha N_{\rm th}\,.$$

To determine the size of the clusters of the metallic phase, the theoretical mean coordination numbers of the first three coordination shells were calculated as a function of the cluster radius $R_{\rm c}$, under the hypothesis of a spherical fcc shape.

The experimental N values were divided by the calculated ones [22] so achieving an extimation of $\alpha(R)$ as a function of $R_{\rm c}$ (Fig. 6). In the absence of errors, the three curves obtained for the three shells should intersect when $R_{\rm c}$ is equal to the actual dimension of the clusters. Taking into account the errors, we obtained two curves for each shell; all curves define an overlap region in the 7.5 Å $< R_{\rm c} <$ 9.5 Å range. The mean diameter so determined is at least a factor two lower than the value of $D = 35$ Å found in the monometallic Ag sample.

In order to control in the bimetallic pumice-supported samples if we are really dealing with monometallic clusters or alloyed Ag-Pd clusters, since Ag and Pd have similar backscattering amplitudes but very different interatomic distances values a higher sensitivity can be achieved using the R values. It is known that in fcc binary metallic alloys Vegard's law, which states that the mean lattice pa-

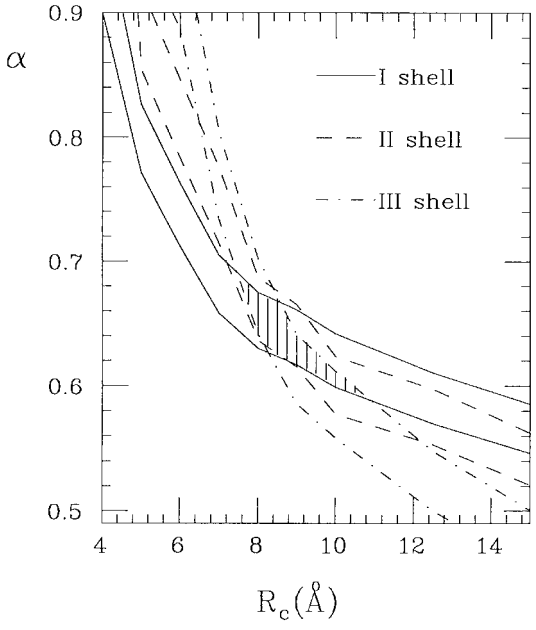

Fig. 6. Ratio (α) of the experimental N values of sample **A** and the theoretical ones as a function of the cluster radius, R_c.

rameter varies linearly with the composition, is not valid. According to reference [28], for a sample which presents a 1:5 ratio between Ag:Pd the R value predicted is of about 2.78 Å. Such theoretical value is calculated for bulk samples and not for clusters; since the Pd clusters have mean sizes around 50 Å we consider that at least for Pd, the bulk approximation must be valid. The experimental values we achieved are 2.75 Å at the Pd K-edge and 2.83 Å at the Ag one. At the Pd K-edge, the R values of the three Ag-Pd samples are exactly the values found in the Pd bulk and in the pumice-supported monometallic Pd reference sample so we can conclude that there is no evidence of alloying. At the Ag K-edge, the R_1 values found show a 2% contraction with respect to the reference samples (2.83 Å instead of 2.87 Å). Contractions were found also for the second (R_2) and third (R_3) shells interatomic distances. The ratios $R_2/R_1 = 1.40$ and $R_3/R_1 = 1.73$ are still the ones expected for a fcc structure. The contraction observed can be due to the small cluster dimensions as already observed in small Ag cluster with mean diameters lower than 25 Å [29] and in other noble-metal clusters [30, 31]. In order to explain the reduced Pd cluster dimension as the Ag amount increases, we can suppose that a part of the Ag clusters sits on the surface of the Pd ones, giving rise to some alloying only in the boundary regions. In this case the observed contraction will partially be given also by this effect.

In the results obtained from the WAXS data analysis (Tab. 4) a strict similarity between the ones at λ_{off} and λ_{Ag} can be seen. This shows that the Ag contribution is not relevant. Furthermore, the evident decrease of the scattering intensity at λ_{Pd} and the ratio of the two components that is nearly constant for the three different wavelengths, suggests that the investigated (111) peak is mostly attributable to Pd scattering atoms. As a consequence, it is possible to state that a bimodal Pd crystallites size distribution is present, with mean dimensions of about 32 Å and 172 Å, respectively. On the other hand, no evidence of Ag clusters was found, probably due to their small dimensions.

The absence of any recognizable structure in the DAWAXS pattern corresponding to the λ_{Ag}-λ_{off} couple confirms this result. The size distribution corresponding to a Lorentzian peak profile is exponential, as can be calculated from the second derivative of the peak profile Fourier Transform [20]. In the present case, we have therefore a size distribution coming from (if other effects, like instrumental or disorder ones, can be neglected) the superposition of two different exponential size distributions. It looks likely that, owing to the relatively high temperature of preparation and to the small specific surface area of the carrier, the larger size component comes from those particles that were close enough to undergo coalescence during the catalyst preparation.

It is evident that the cluster dimension observed by XAFS has a correspondence only with one of the two components measured by WAXS. XAFS, in the presence of a cluster size distribution, measures an average dimension weighted by the fraction of atoms corresponding to each size. If we assume the existence, in sample **A**, only of a bimodal distribution, as measured by WAXS, we should have evaluated, from the XAFS coordination numbers, a cluster dimension of about 50 Å instead of 30 Å. The mismatch probably arises because WAXS cannot reveal the presence of cluster dimensions lower than 20 Å: to find an agreement between the results of the two techniques we must assume the presence of a relevant fraction of clusters with mean dimensions ≤ 20 Å.

Finally, it is worth noticing that the cell constant corresponding to the lower-size Pd population is larger than that pertaining to the thicker component by about 0.01 Å. This value could give a hint of a Pd-Ag interaction, besides the already discussed correlation existing between the Pd cluster size and the Pd-Ag relative content. A possible explanation of the observed phenomena could be that a segregation of Ag atoms at the surface of the Pd clusters both hinders the Pd growth and gives rise to an expanded cell constant, more evident, for the higher influence of the surface effects, on the smaller Pd crystallites. However it cannot be excluded that, as already observed [32], a slight expansion of the lattice parameter in the [111] direction could be also given by the presence of small Pd clusters.

5 Conclusions

The synthesis technique used in the preparation of the pumice-supported Ag-Pd catalysts led to the formation of monometallic Ag and Pd clusters since no direct evidence of alloying of both metal components was found. XAFS data analysis revealed the presence of Pd clusters whose mean dimensions are related to the amount of Ag present in the sample and has shown that silver is partially dispersed in the support bonding oxygen atoms and partially aggregated in small metal clusters ($D < 20$ Å). AWAXS

data analysis has shown no evidence of Ag clusters, probably due to their small dimensions but has revealed a possible interaction of Ag atoms and/or clusters segregated at the surface of the Pd clusters.

GILDA is financed by the Italian institutions CNR, INFM and INFN. The financial support of CNR (Progetto finalizzato MSTA II) is gratefully acknowledged.

References

1. J.P. Boitiaux, J. Cosyns, M. Derrien, G. Leger, Hydrocarb. Processing March issue (1985) 51.
2. V. Ponec, G.C. Bond, Stud. Surf. Sci. Catal. **95**, 491 (1995).
3. A. Borgna, B. Moraweck, J. Massardier, A.J. Renouprez, J. Catal. **128**, 99 (1991).
4. A. Sarkany, Z. Zsoldos, B.K. Furlong, J.W. Hightower, L. Guczi, J. Catal. **141**, 566 (1993).
5. H. Remita, J. Khatouri, M. Tréguer, J. Amblard, J. Belloni, Z. Phys. D **40**, 127 (1997).
6. L. Tröger, H. Hunnefeld, S. Nunes, M. Oehring, D. Fritsch, Z. Phys. D **40**, 65 (1997).
7. M. Meyer, N. Barbouth, J. Oudart, C. R. Acad. Sci. (Paris) Ser. II Mec. Phys. Chem. Sci. **311**, 313 (1990).
8. G.C. Bond, A.F. Rawle, J. Mol. Catal. **109**, 261 (1996).
9. G. Deganello, L.F. Liotta, A. Longo, A. Martorana, Y. Yanev, N. Zotov, J. Non-Cryst. Solids **232**, 547 (1998).
10. G. Deganello, D. Duca, A. Martorana, A. Benedetti, G. Fagherazzi, J. Catal. **150**, 127 (1994).
11. A. Balerna, S. Coluccia, G. Deganello, A. Longo, A. Martorana, G. Martra, C. Meneghini, P. Pertici, G. Pipitone, E. Pitzalis, A.M. Venezia, A. Verrazzani, G. Vitulli, in preparation.
12. A.M. Venezia, A. Parmaliana, A. Mezzapica, G. Deganello, J. Catal. **172**, 463 (1997).
13. L.F. Liotta, A.M. Venezia, A. Martorana, G. Deganello, J. Catal. **171**, 177, (1997).
14. S. Pascarelli, F. D'Acapito, G. Antonioli, A. Balerna, F. Boscherini, R. Cimino, G. Dalba, P. Fornasini, G. Licheri, C. Meneghini, F. Rocca, S. Mobilio, ESRF Newslett. **23**, 17 (1995).
15. S. Pascarelli, F. Boscherini, F. D'Acapito, J. Hrdy, C. Meneghini, S. Mobilio, J. Synch. Rad. **3**, 147 (1996).
16. A.N. Fitch, in *European Powder Diffraction Conference: EPDIC IV, Materials Science Forum* **228**, 219 (1996).
17. A. Filipponi, A. Di Cicco, C.R. Natoli, Phys. Rev. B **52**, 15122 (1995).
18. A. Filipponi, A. Di Cicco, Phys. Rev. B **52**, 15135 (1995).
19. P. Thompson, D.E. Cox, L.B. Hastings, J. Appl. Cryst. **20**, 79 (1987).
20. S. Ciccariello, Acta Cryst. A **46**, 175 (1990).
21. S. Enzo, G. Fagherazzi, A. Benedetti, S. Polizzi, J. Appl. Cryst. **21**, 536 (1988).
22. M. Borowski, J. Phys. IV **7**, C2-259 (1997).
23. J. Zhao, P.A. Montano, Phys. Rev. B **40**, 3401, 1989 (Rapid Communication).
24. B.S. Clausen, H. Topsoe, L.B. Hansen, P. Stoltze, J.K. Norskov, Jpn J. Appl. Phys. **32**, Suppl. 32-2, 95 (1993).
25. F. D'Acapito, Ph. D. thesis, University of Grenoble I, 1997.
26. G. Dalba, P. Fornasini, F. Rocca, E. Bernieri, E. Burattini, S. Mobilio, J. Non-Cryst. Solids **91**, 153 (1987).
27. J.B.A.D. van Zon, D.C. Koningsberger, H.F.J. vant Blik, R. Prins, D.E. Sayers, J. Chem. Phys. **82**, 5742 (1985).
28. N. Mousseau, M.F. Thorpe, Phys. Rev. B **45**, 2015 (1992).
29. P.A. Montano, W. Schulze, B. Tesche, G.K. Shenoy, T.I. Morrison, Phys. Rev. B **30**, 672 (1984).
30. R. Lamber, S. Wetjen, N.I. Jaeger, Phys. Rev. B **51**, 10968 (1995).
31. A. Balerna, E. Bernieri, P. Picozzi, A. Reale, S. Santucci, E. Burattini, S. Mobilio, Phys. Rev. B **31**, 5058 (1985).
32. P. Jiang, F. Jona, P.M. Marcus, Phys. Rev. B **36**, 6336 (1987).